Polar Geosci., **15**, 17-36, 2002
© 2002 National Institute of Polar Research

SHRIMP geochronology of a mylonite zone on Tonagh Island: characterisation of the last high-grade tectonothermal event in the Napier Complex, East Antarctica

Warwick A. Crowe[1], Yasuhito Osanai[2], Tsuyoshi Toyoshima[3], Masaaki Owada[4], Toshiaki Tsunogae[5] and Tomokazu Hokada[6]

[1]*Tectonics Special Research Centre, Department of Geology and Geophysics, University of Western Australia, 35 Stirling Hwy Crawley, WA 6009, Australia*
[2]*Department of Earth Sciences, Okayama University, Tsushima-naka 3-chome, Okayama 700-8530*
[3]*Graduate School of Science and Technology, Niigata University, Ikarashi, Niigata 950-2181*
[4]*Department of Earth Sciences, Yamaguchi University, Yoshida 1677-1, Yamaguchi 753-8512*
[5]*Institute of Geoscience, The University of Tsukuba, Tsukuba 305-8571*
[6]*Department of Geology, National Science Museum, Shinjuku-ku, Tokyo 169-0073*

Abstract: Tonagh Island within the highest-grade zone of the Napier Complex, East Antarctica, consists of a strongly layered sequence of quartzofeldspathic gneiss, mafic granulite and ultramafic gneiss subdivided into five lithostratigraphic units by major NE-SW to E-W trending steeply-dipping D_6 shear zones. D_6 shear zones cut the principal foliation defined by D_1 and D_2 structures associated with the ultrahigh-temperature metamorphism. Zircons from two mylonite samples with moderate NE pitching mineral lineations within a D_6 shear zone and a D_6 mylonite and ultramylonite sample from within high strain zones that have an overprinting sub-horizontal mineral lineation were analyzed. All samples have anhydrous mineral assemblages with a late textural association of biotite, which formed pre- to syn- a secondary overprinting high temperature mylonitic fabric. Zircons in all samples contain a structureless zone that constitutes most of the grain area and commonly have a relict discordant, oscillatory-zoned core. The core may be obscured to the extent where only a structureless or an indistinct remnant remains These internal patterns are consistent with recrystallisation and annealing processes resulting in resetting of the U-Pb system during mylonitsation involving possibly three events between *ca.* 2550 Ma and *ca.* 2470 Ma. The timing of D_6 mylonitisation between *ca.* 2470-2550 Ma on Tonagh Island requires an earlier timing for UHT metamorphism. This is consistent with regional models that attribute UHT metamorphism to pre- *ca.* 2550 Ma tectonothermal events in the Napier Complex.

key words: Napier Complex, Tonagh Island, SHRIMP geochronology, mylonite

1. Introduction

The Archaean to Paleoproterozoic Napier Complex of East Antarctica is distinguished by ultra-high temperature (UHT) granulite facies rocks which include garnet and pyroxene-bearing quartzofeldspathic orthogneiss with subordinate paragneiss and mafic gneiss (Sheraton *et al.*, 1987). The highest-grade region in the west of the Napier Complex is characterised by mineral assemblages with sapphirine and quartz-spinel, quartz-orthopyroxene-sillimanite and quartz-osumilite (Dallwitz, 1968; Ellis, 1980; Grew, 1980; Harley, 1985; Sheraton *et al.*, 1987; Motoyoshi *et al.*, 1990) with *P-T* conditions of 8–10 kb and 1000–1120°C (Harley and Hensen, 1990; Harley, 1998; Harley and Motoyoshi, 2000).

Three major tectonothermal events defined within the Napier Complex are characterised by a pervasive low-angle lineated gneissocity (D_1) folded by tight recumbent to inclined folds (D_2) and refolded by kilometre scale upright to inclined open folds (D_3) resulting in regional dome and basin structures (James and Black, 1981; Sheraton *et al.*, 1987). Considerable debate exists on the interpretation and geological significance of the available geochronological data in terms of this tectonothermal history. Initially the timing of UHT metamorphism was correlated with a protracted episode from D_1 at *ca.* 3100 Ma to D_2 at *ca.* 2900 Ma (Black and James, 1983; Black *et al.*, 1983, 1986; Sheraton *et al.*, 1987). More recently Harley and Black (1997), using new SHRIMP U-Pb zircon ages, proposed that UHT metamorphism occurred at *ca.* 2850–2820 Ma in the western Napier Complex overprinting a more wide spread 2980 Ma D_1-M_1 lower *P-T* granulite facies event. A protracted D_3-M_3 event between 2455–2480 Ma followed, associated with considerable isotopic resetting and new zircon growth. Still more recently further SHRIMP data on leucosomes constrain UHT metamorphism to be older than *ca.* 2550–2590 Ma but is considered to be younger than *ca.* 2980 Ma (Harley *et al.*, 2001). In contrast, others consider the predominant isotopic imprint at *ca.* 2450–2500 Ma to represent the timing of high-grade metamorphism (*e.g.* Grew and Manton, 1979; DePaolo *et al.*, 1982; Sandiford and Wilson, 1984; Owada *et al.*, 1994; Asami *et al.*, 1998; Carson *et al.*, In Press a and b).

Given the continuing controversy regarding the tectonothernal significance of the *ca.* 2500 Ma D_3-M_3 event, SHRIMP analysis of zircon from four samples from within a mylonite zone on Tonagh Island was undertaken with the aim of determining the timing of mylonitisation which represents the last major ductile deformation event on Tonagh Island. The mylonite samples are from one of a series of major NE-SW to E-W trending D_6 mylonite zones on Tonagh Island which have been well constrained within a relative structural sequence by Toyoshima *et al.* (1999).

2. Geology and deformation of Tonagh Island

Tonagh Island is in the SE of Amundsen Bay at the northern extent of the Scott Mountains chain and within the highest-grade zone of the Napier Complex (Fig. 1). Orthopyroxene-bearing and garnet-bearing quartzofeldspathic gneiss are the principal lithologies within a strongly layered succession (Osanai *et al.*, 1999, 2001). The succession also includes two-pyroxene mafic granulite, garnet-orthopyroxene gneiss and granulite,

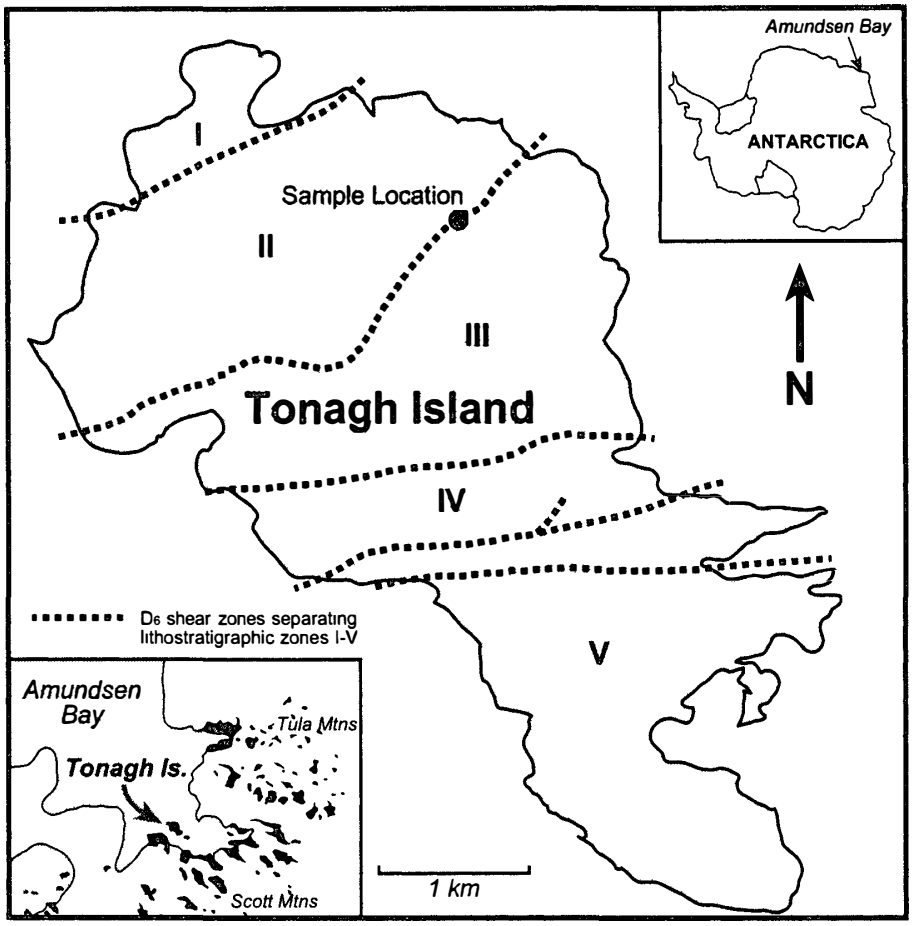

Fig. 1. The position of D_6 shear zones that separate five lithostratigraphic zones and the sample location on Tonagh Island.

magnetite-quartz gneiss, metamorphosed ultramafic rocks, two series of layered mafic gneiss with orthopyroxene-bearing or garnet-bearing quartzofeldspathic gneiss and unmetamorphosed dolerite and granitic pegmatite (Osanai *et al.*, 1999, 2001). Protolith to the layered metamorphic rocks was inferred by Osanai *et al.* (1999) to be an Archaean greenstone succession, which is supported by komatiitic geochemical affinities of some ultramafic units (Owada *et al.*, 1999). Five lithostratigraphic units are distinguished and separated by major NE-SW to E-W trending shear zones (Osanai *et al.*, 1999; Fig. 1). These are D_6 shear zones, characterised by steeply NW to N dipping thick mylonite zones consisting principally of anhydrous mineral assemblages and associated with both foliated and unfoliated pseudotachylite (Toyoshima *et al.*, 1999; Table 1).

The D_6 mylonite cuts all previous structures including a weak D_1 foliation associated with the UHT metamorphism and the pervasive dextral reverse, layer parallel shearing of D_2, the principal foliation and lineation forming event (Toyoshima *et al.*, 1999). The D_3 event is a progressive shearing event from D_2 with strain localised along thin mylonite and pseudotachylite zones and D_4 and D_5 represent open orthogonal fold events associated with E-W and N-S shortening respectively (Toyoshima *et al.*, 1999). Subsequent post-D_6 deformation involved brittle faulting and intrusion of pegmatite and dolerite (Toyoshima *et al.*, 1999).

Table 1. Summary of the tectonic history on Tonagh Island after Toyoshima et al. (1999).

Stage	Deformation	Metamorphism	Regional Events
D_1	Weak layer parallel S_1 foliation and very weak lineation/boudinage.	Prograde metamorphism (UHT) and anatexis.	D_1-M_1
D_2	Moderately NW dipping S_2 foliation associated with layer parallel shearing and strong mineral lineation, intrafolial folds.	Initiation of retrograde amphibolite facies metamorphism.	D_2-M_2
D_3	Thin shear zones parallel to sub-parallel with S_2, mylonite and pseudotachylite development.	Retrograde granulite facies metamorphism	
D_4	N-S trending upright open to gentle folds.		
D_5	WNW-ESE to E-W trending upright tight to open folds.	Retrograde metamorphism	D_3-M_3
D_6	Thick mylonite zones trend NE-SW to E-W and dip steeply to N to NW define major unit boundaries. Mylonite and pseudotachylite development	Retrograde granulite facies metamorphism.	
D_7-D_9	Brittle faulting (minor mylonite development) and emplacement of pegmatite and dolerite dykes	Retrograde amphibolite facies metamorphism	

The D_6 shear zones are characterised by a complex polyphase reactivation history possibly involving a sequence of reverse to dextral-reverse shearing and discrete high-strain sinistral to sinistral-normal shear zones and later dextral shearing (Toyoshima *et al.*, 1999). Subsequent brittle deformation and pseudotachylite development was overprinted by late mylonite associated with reverse shearing, followed by further normal brittle faulting and pseudotachylite formation (Toyoshima *et al.*, 1999).

Peak metamorphic conditions determined for aluminous gneisses on Tonagh Island where 0.8–1.1 GPa at 1030–1100°C (Hokada *et al.*, 1999). A low temperature isobaric cooling event (at 650–700°C and 6.5–8.0 kb) recorded in mafic gneiss is distinct from the isobaric cooling at high-grade conditions of *ca.* 950°C prevalent through the western Napier Complex (Tsunogae *et al.*, 1999).

3. Sample petrography

Four samples from a D_6 mylonite zone on Tonagh Island were analysed (Fig. 1). Two samples, W98021101B and W98021101C2a, are from relatively low-strain areas within the mylonite with moderate NE pitching mineral lineations. Sample W98021101C2a contains discrete micro-scale high strain zones associated with deformation and recrystallisation of pseudotachylite. The remaining two samples (W98021101D2 and W98021102A) are a mylonite and ultramylonite from within high strain zones that exhibit an overprinting sub horizontal mineral lineation.

3.1. Orthopyroxene quartzofelspathic mylonite (W98021101B)

The orthopyroxene quartzofeldspathic mylonite sample (W98021101B) has a foliation

defined by zones of plagioclase and K-feldspar with irregular to poor granoblastic texture separated by quartz bands (ribbon quartz). Post-dynamic recrystallisation growth of quartz is exemplified by rounded and embayed grain contacts, which locally, overgrow or include feldspar, orthopyroxene and opaque oxides. Orthopyroxene is xenoblastic with sub-rounded to angular grain margins. The larger grains have a preferred alignment parallel to the foliation. These larger crystals are commonly fractured and fragments may be transposed along the foliation. Only locally is fine recrystallised orthopyroxene recognised on grain margins. Small round opaque oxides are present as inclusions within orthopyroxene, whereas larger rounded to subangular grains are embayed and intergrown with orthopyroxene. Minor phases include apatite, clinopyroxene, and biotite. Biotite is characteristically present on grain margins of orthopyroxene, along fractures associated with localised alteration of orthopyroxene, and on opaque oxides.

3.2. Orthopyroxene garnet quartzofeldspathic mylonite (W98021101C2a)

The principal foliation within the orthopyroxene-garnet quartzofeldspathic mylonite is defined by bands of recrystallised quartz which have undulose to banded extinction and separate zones of recrystallised K-feldspar and plagioclase. The recrystallised feldspars have undulose to mottled extinction, indicative of subgrain development, and are surrounded by a mortar of fine-grained tertiary recrystallised feldspar. Relict porphyroclasts of mesoperthite and orthopyroxene are subrounded and mantled typically by fine-grained recrystallised phases which also line fractures and broken surfaces of the porphyroclasts. Exsolution lamellae within mesoperthite porphyroclasts are commonly bent and locally display mottled extinction textures on the crystal margins, consistent with subgrain development. Fine-grained biotite occurs sparsely through the tertiary recrystallised feldspar and is abundant in foliated pseudotachylite which is characterised by fine-grained, sharply-bounded zones that branch into discordant vein-like zones (*cf.* Toyoshima *et al.*, 1999). The foliation in these zones is parallel with the principal mylonitic foliation and is defined by a strong biotite orientation and compositional layering of biotite, feldspar, garnet and orthopyroxene. These foliated zones truncate some of the branching discordant zones which show a poor preferred alignment of biotite. The garnets within the foliated pseudotachylite zones are idiomorphic and contain fine inclusions of biotite. Garnet also occurs as a fine-grained mortar on orthopyroxene and forms distinct bands within orthopyroxene-rich layers. Larger garnets within these zones contain biotite as inclusions and as coarse-grained fracture fills. Rare small rounded orthopyroxenes with biotite altered margins also occur as inclusions in garnet.

3.3. Orthopyroxene, quartzofeldspathic mylonite (W98021101D2)

The orthopyroxene, quartzofeldspathic mylonite is from a thin discrete high strain zone with a shallow SW pitching mineral lineation. Recrystallised trails of orthopyroxene and zones of recrystallised feldspar with localised bands of comparatively coarse-grained recrystallised quartz define a strong pervasive foliation. A mortar of fine-grained recrystallised feldspar mantles sub-rounded porphyroclasts of plagioclase and K-feldspar which have undulose to mottled extinction consistent with sub-grain development. Elongate porphyroclasts of orthopyroxene are mantled typically by fine-grained recrystallised orthopyroxene that forms aggregate trails along the foliation defining a compositional layering.

Other minor porphyroclast phases include clinopyroxene and apatite. Fine-grained biotite is present along recrystallised orthopyroxene-rich layers, in the pressure shadows of porphyroclasts, and along fracture surfaces in porphyroclasts. Fine-grained opaque oxide has a similar late textural association as biotite plus an earlier phase is present as inclusions within orthopyroxene and plagioclase.

3.4. Orthopyroxene,garnet ultramylonite (W98021102A)

Sample W98021102A is from a 6–10 cm wide ultramylonite band with a shallow W pitching mineral lineation. A compositional layering is defined by zones of recrystallised quartz, feldspar and biotite interbanded with zones rich with recrystallised orthopyroxene biotite, opaque oxide and garnet. Porphyroclasts of orthopyroxene are typically lensoidal in shape and aligned parallel to the foliation. Recrystallised grains mantle these porphyroclasts and trail along the foliation. Feldspar porphyroclasts, which consist of plagioclase, K-feldspar, and rare mesoperthite, are rounded and commonly show undulose to a mottled extinction. Garnet porphyroclasts are less common and have associated recrystallised mantles that are not as prominently developed as those on orthopyroxene porphyroclasts. Biotite is present throughout the sample and shows a strong preferred alignment parallel to the main mylonitic foliation and is concentrated along zones with abundant orthopyroxene. Fine-grained biotite is also present along grain boundaries and as inclusions within recrystallised quartz and feldspar zones that exhibit a poorly preserved granoblastic texture with irregular and curved grain boundaries. Inclusions of biotite and opaque oxides are present within garnet. Locally, relatively coarse-grained undeformed biotite occurs along fracture surfaces in garnet.

4. Sample preparation and analytical procedures

Zircons were separated by conventional crushing, sieving, heavy liquid and magnetic procedures and mounted in epoxy disks with zircon U-Pb standard (CZ3), polished and gold coated prior to analysis. U-Pb analysis on selected zircons was carried out using the SHRIMP II ion microprobe at Curtin University, Perth, Australia. Instrument operating procedures and conditions are outlined by Nelson (1997).

Inter-element discrimination in the Pb/U isotopic ratios were corrected for by reference to the linear calibration of $^{206}Pb^{+}/^{238}U^{+}$ to $^{254}UO^{+}/^{238}U^{+}$ for the CZ3 zircon standard ($^{206}Pb/^{238}U = 0.0914$) (Nelson, 1997). Common Pb corrections were made using the isotopic composition of Broken Hill common Pb. Most samples had negligible common lead corrections with $f206$ less than 1% (Table 1). Data were reduced using KRILL, a computer program developed by Peter Kinny at Curtin University. Individual SHRIMP analyses are reported with 1σ errors for ^{204}Pb-corrected $^{206}Pb/^{238}U$, $^{207}Pb/^{235}U$ and $^{207}Pb/^{206}Pb$ ratios and $^{207}Pb/^{206}Pb$ ages (Table 2). Calibration errors for U/Pb ratios in the CZ3 standard included for each sample are $\pm 1.67\%$ (W98021101B), $\pm 1.21\%$ (W98021101C2a), $\pm 1.1\%$ (W98021101D2) and $\pm 0.66\%$ (W98021102A). Weighted mean ages for pooled ^{204}Pb corrected $^{207}Pb/^{206}Pb$ ratios are reported with 95% confidence limits.

5. SHRIMP geochronology results

Table 2 list the isotopic data for individual zircon analyses which are plotted on conventional $^{206}Pb/^{238}U$-$^{207}Pb/^{235}U$ concordia diagrams in Figs. 3 to 6.

Zircons extracted for analysis from the four samples are anhedral to subhedral, ranging from rounded grains to subrounded prismatic forms with aspect ratios of 1 : 1.5 to 1 : 3. In back scattered electron (BSE) and cathodoluminescence (CL) images, zircons commonly have subrounded cores that are structureless or show a disrupted or obscured oscillatory zonation, surrounded by a structureless or diffuse broad and patchy banded zircon (Fig. 2). Zonation in cores is truncated by the structureless zircon, which may encroach on the cores as irregular embayed lobes. This truncating structureless zircon, which has a high-CL response and a correspondingly low U concentration and a generally high Th/U ratio, is interpreted to represent recrystallisation of original zircon (*cf.* Pidgeon, 1992; Vavra *et al.*, 1996, 1999; Schaltegger *et al.*, 1999; Fig. 2a, b and e).

Structureless zircon with an intermediate to low CL and a higher BSE response is generally associated with relict euhedral zonation. This shows varying degrees of preserva-

Table 2. Analyses of U, Th and Pb for zircons from samples W98021101B, W98021101C2a, W98021101D2 and W98021102A.

grain-spot	U (ppm)	Th (ppm)	Th/U	f_{206} (%)	206*/238	(±1σ)	207*/206*	(±1σ)	207/206* Age(Ma)	(±1σ)
Sample W98021101B										
1B-12.1	14	43	3.047	1 924	0.4909	± 146	0 1566	± 65	2420	± 71
1B-11 1	10	27	2 711	0 000	0 4996	± 149	0 1700	± 34	2558	± 34
1B-11 2	94	434	4 631	0.137	0 4954	± 90	0 1591	± 13	2446	± 13
1B-11 3	437	491	1 125	0 014	0 5491	± 91	0 1867	± 6	2713	± 5
1B-12 2	102	187	1.831	0 088	0 4914	± 88	0 1668	± 12	2526	± 13
1B-4 1	17	44	2 529	0 265	0.4900	± 130	0 1664	± 37	2522	± 37
1B-4.2	568	112	0 197	0 007	0 5103	± 84	0 1832	± 5	2682	± 5
1B-13 1	11	7	0 606	1 294	0 4307	± 144	0 1522	± 88	2371	± 99
1B-13 2	949	319	0 337	0 023	0 5017	± 82	0 1643	± 4	2500	± 4
1B-14 1	73	84	1 165	0 106	0 4861	± 92	0.1699	± 16	2557	± 16
1B-14 2	2235	560	0 251	0.009	0 4949	± 80	0 1623	± 2	2479	± 2
1B-15 1	15	50	3 257	0 662	0 4717	± 124	0 1512	± 56	2359	± 63
1B-15 2	274	518	1 889	0 000	0 4737	± 79	0 1639	± 6	2497	± 7
1B-16 1	5	8	1 381	0 000	0 3846	± 166	0 1652	± 45	2510	± 45
1B-16 2	185	192	1 035	0 005	0 5213	± 88	0.1847	± 8	2696	± 7
1B-8 1	214	520	2 433	0 045	0 4912	± 83	0 1700	± 8	2558	± 8
1B-8 2	6	5	0.792	0 000	0 4887	± 180	0 1599	± 53	2454	± 56
1B-7 1	173	426	2 469	0 452	0 4703	± 81	0 1617	± 11	2473	± 12
1B-7 2	853	494	0 578	0 004	0 5060	± 82	0 1846	± 4	2694	± 3
1B-10 1	931	730	0 784	0 010	0 4837	± 79	0 1744	± 4	2600	± 4
1B-10 2	47	10	0 203	0 720	0 4619	± 102	0 1681	± 31	2539	± 31
1B-9 1	262	345	1.318	0 027	0 4724	± 80	0 1616	± 7	2472	± 7
1B-9 2	292	246	0 842	0 021	0 5438	± 91	0 1865	± 7	2712	± 7
1B-17 1	240	177	0 736	0 031	0 4962	± 84	0 1701	± 8	2559	± 8
1B-17 2	26	121	4 625	0 478	0 4307	± 103	0 1643	± 43	2500	± 44
Sample W98021101C2a										
C2a-1 1	193	317	1 639	0 000	0 4833	± 61	0 1667	± 8	2524	± 8
C2a-1 2	127	100	0 786	0 010	0 4714	± 64	0 1619	± 12	2475	± 12
C2a-3 1	197	145	0 734	0 093	0 4570	± 63	0 1618	± 15	2474	± 15
C2a-3 2	653	336	0 515	0 011	0 4466	± 52	0 1638	± 5	2496	± 5
C2a-5 1	776	149	0 192	0 027	0 4709	± 54	0 1613	± 4	2469	± 4
C2a-5 2	106	97	0 920	0 139	0 4949	± 69	0 1699	± 15	2557	± 15
C2a-6 1	2038	713	0 350	0 000	0 5039	± 57	0 1770	± 2	2625	± 2

Table 2. Continued.

grain-spot	U (ppm)	Th (ppm)	Th/U	f_{206} (%)	206*/238	(±1σ)	207*/206*	(±1σ)	207/206 Age(Ma)	(±1σ)
Sample W98021101C2a *Cont.*										
C2a-6 2	1188	113	0 095	0.000	0 4618	± 53	0 1639	± 4	2496	± 4
C2a-7 1	3746	277	0 074	0 000	0 4711	± 53	0 1568	± 2	2421	± 2
C2a-7 2	770	65	0 085	0 023	0 4698	± 54	0 1650	± 4	2508	± 4
C2a-7 3	108	98	0 909	0 023	0 4883	± 66	0 1671	± 11	2529	± 11
C2a-16 1	856	407	0 475	0 032	0 4580	± 53	0 1643	± 6	2501	± 6
C2a-16 2	614	239	0 390	0 006	0 4853	± 58	0 1750	± 8	2606	± 7
C2a-4 1	3248	1009	0 310	0 002	0 4657	± 53	0 1615	± 2	2471	± 2
C2a-10 1	744	353	0 474	0 011	0 4745	± 55	0 1656	± 4	2513	± 4
C2a-10 2	2400	1830	0 763	0 004	0 4671	± 53	0 1650	± 2	2508	± 2
C2a-12 1	312	139	0 445	0 090	0 4787	± 58	0 1626	± 7	2482	± 7
C2a-12 2	178	262	1 470	0 000	0 4761	± 61	0 1640	± 8	2497	± 8
C2a-13 1	793	446	0 563	0 000	0 4860	± 57	0 1659	± 4	2516	± 4
C2a-13 2	1287	474	0 368	0 002	0 4601	± 52	0 1627	± 3	2484	± 3
C2a-13 3	1248	415	0 333	0 010	0 4643	± 53	0 1640	± 3	2497	± 3
Sample W98021101D2										
D2-5 1	51	112	2 175	0 142	0.4632	± 81	0 1622	± 25	2479	± 26
D2-5 2	78	199	2 552	0 000	0 4737	± 68	0 1620	± 14	2476	± 15
D2-4 1	340	304	0 895	0 029	0 4862	± 53	0 1695	± 7	2553	± 7
D2-4 2	1725	287	0 166	0 002	0 4565	± 45	0 1642	± 3	2499	± 4
D2-1 1	1097	689	0 628	0 030	0 5006	± 50	0 1733	± 4	2589	± 4
D2-1 2	135	164	1 210	0 021	0 4603	± 60	0 1644	± 14	2501	± 14
D2-11 1	1746	654	0 374	0 064	0 4343	± 43	0 1651	± 4	2509	± 4
D2-11 2	353	280	0 793	0 055	0 4431	± 49	0 1693	± 9	2551	± 9
D2-11 3	1939	322	0 166	0 016	0 4966	± 48	0 1829	± 4	2679	± 3
D2-13 1	1147	685	0 597	0 024	0 4735	± 47	0 1655	± 4	2513	± 4
D2-13 2	86	209	2 431	0 305	0 4627	± 75	0 1620	± 20	2476	± 21
D2-14 1	333	425	1 276	0 034	0 5036	± 56	0 1824	± 8	2674	± 7
D2-14 2	148	163	1 099	0 131	0 4701	± 63	0 1624	± 13	2481	± 14
D2-20 1	927	416	0 449	0 058	0 4776	± 48	0 1711	± 5	2569	± 5
D2-20 2	488	414	0 849	0 062	0 4597	± 49	0 1660	± 7	2518	± 7
D2-19 1	1623	280	0 173	0 009	0 4562	± 45	0 1653	± 4	2511	± 4
D2-19 2	458	359	0 783	0 039	0 4523	± 48	0 1619	± 7	2475	± 7
D2-5 3	50	95	1 907	0 000	0 5254	± 99	0 1810	± 23	2662	± 21

tion from a "ghost" out-line of zonation to well defined euhedral zoning that may show only a patchy diminished definition (Figs. 2c, f, i, m, n and o). These features have been attributed to annealing processes that involve a solid-state reorganisation of the lattice caused by differential α-decay between distinct U and Th composition growth zones (Schaltegger *et al.*, 1999). Characteristic products of this process are partial preservation of textural and primary Th/U ratios (Schaltegger *et al.*, 1999).

The U and Th concentrations for structureless to disrupted euhedrally zoned zircon are variable and show no correlation with degree textural preservation. The Th/U ratios are also significantly variable, up to nearly 5 in sample W98021101.B. Only sample W98021102.A show a more restricted Th/U ratio values below 0.8. Most grains also show a thin sharply defined structureless overgrowth rim.

The concordance of the data for these samples suggests recrystallisation and annealing at *ca.* 2500 Ma has resulted in near complete Pb-loss and resetting of the U-Pb system. Complete Pb-loss and resetting associated with recrystallisation and annealing processes are described by Vavra *et al.* (1996; 1999), Gebauer *et al.* (1997) and Schaltegger *et al.* (1999). Some zircons show incongruent apparent $^{207}Pb/^{206}Pb$ ages (outside σ1 limits) between core

Table 2. Continued.

grain-spot	U (ppm)	Th (ppm)	Th/U	f_{206} (%)	206*/238	(±1σ)	207*/206*	(±1σ)	207/206* Age(Ma)	(±1σ)
Sample W98021101D2 *Cont.*										
D2-7.1	145	165	1.134	0.050	0.4790	± 60	0 1637	± 12	2495	± 12
D2-12 1	215	122	0 566	0 045	0.5080	± 59	0 1818	± 11	2669	± 10
D2-12.2	274	179	0 655	0.063	0.4739	± 54	0 1619	± 9	2475	± 9
D2-12 3	396	475	1 200	0.077	0.5112	± 55	0 1829	± 7	2680	± 6
Sample W98021102A										
A-7.1	160	76	0 472	0.067	0 5202	± 47	0 1781	± 13	2636	± 12
A-7 2	260	92	0 353	0.000	0 4966	± 37	0 1676	± 9	2534	± 9
A-10 1	742	5	0 006	0.002	0 5237	± 27	0.1842	± 6	2691	± 6
A-10 2	452	57	0.126	0 064	0 5203	± 30	0.1798	± 7	2651	± 7
A-3.1	218	81	0 372	0 000	0 4245	± 32	0 1474	± 9	2316	± 10
A-3.2	362	82	0.226	0.058	0 4717	± 30	0.1583	± 7	2438	± 8
A-1.1	1335	18	0.013	0.000	0 5101	± 22	0 1815	± 4	2666	± 3
A-1 2	609	35	0.057	0 000	0 4803	± 25	0 1636	± 5	2493	± 5
A-11 1	449	84	0.188	0.040	0 4614	± 27	0.1553	± 7	2405	± 7
A-11 2	185	121	0 655	0.000	0 4887	± 38	0 1613	± 10	2470	± 11
A-13 1	458	158	0.346	0.012	0 5187	± 30	0.1803	± 7	2656	± 6
A-13.2	901	142	0.158	0.000	0.4621	± 22	0.1603	± 5	2458	± 5
A-18.1	203	144	0.711	0 030	0 5851	± 45	0 2109	± 11	2913	± 8
A-18.2	403	29	0.072	0.053	0 5053	± 30	0.1737	± 7	2594	± 7
A-19.1	205	69	0 335	0.077	0 5345	± 40	0.1855	± 10	2703	± 9
A-19.2	582	19	0.033	0.018	0 4882	± 25	0 1754	± 6	2609	± 6
A-21.1	331	24	0.072	0.009	0 4689	± 29	0 1553	± 8	2405	± 8
A-21.2	205	115	0 561	0.043	0 4899	± 42	0.1648	± 11	2506	± 11
A-17.1	204	110	0.537	0.194	0 5325	± 41	0.1970	± 12	2801	± 10
A-17.2	881	26	0.030	0.006	0 5307	± 26	0 1815	± 5	2667	± 5
A-2 1	2240	115	0 051	0 015	0 4338	± 18	0 1601	± 4	2457	± 4
A-8 1	554	14	0 025	0.013	0 4942	± 27	0 1738	± 6	2595	± 6

^{204}Pb corrected data. f_{206} = the proportion of common ^{206}Pb in measured $^{206}Pb_{Total}$.
$^{206}Pb/^{238}U$ calibration uncertainties (1σ): W98021101B = 1.67%; W98021101C2a = 1.21%; W980201D2 = 1.1%; W980201102A = 0.66%

and rim indicating preferential Pb-loss has occurred in the core (*e.g.* Fig. 2g and k). These cores are typically structureless and the associated analyses yield concordant younger ages consistent with ages from structureless and disrupted zoned rims from other grains. Pb-loss in these cores may have been facilitated by fracturing and the presence of a fluid phase as is suggested by the healed fracture network pattern and age association for the zircon in Fig. 2j and the new zircon growth and associated recrystallisation along a fractured surface of the zircon in Fig. 2d.

5.1. Orthopyroxene quartzofeldspathic mylonite (W98021101B)

A total of 25 SHRIMP analyses yield concordant to near concordant and a number of slightly reversely concordant ages that define two age groups for which no weighted mean ages can be calculated (Fig. 3). The main data group are spread between *ca.* 2550 and 2480 Ma and possibly comprise three distinct age components defined on probability frequency diagrams (Fig. 3 inset). Analyses that make up this group are from recrystallised zircon and from relict cores that are structureless or preserve a disrupted euhedral zoning. Younger analyses and some of the most positively and reversely discordant analyses are defined by low precision data resulting from very low U contents. Most of these analyses are from the low U recrystallised outer zone zircon.

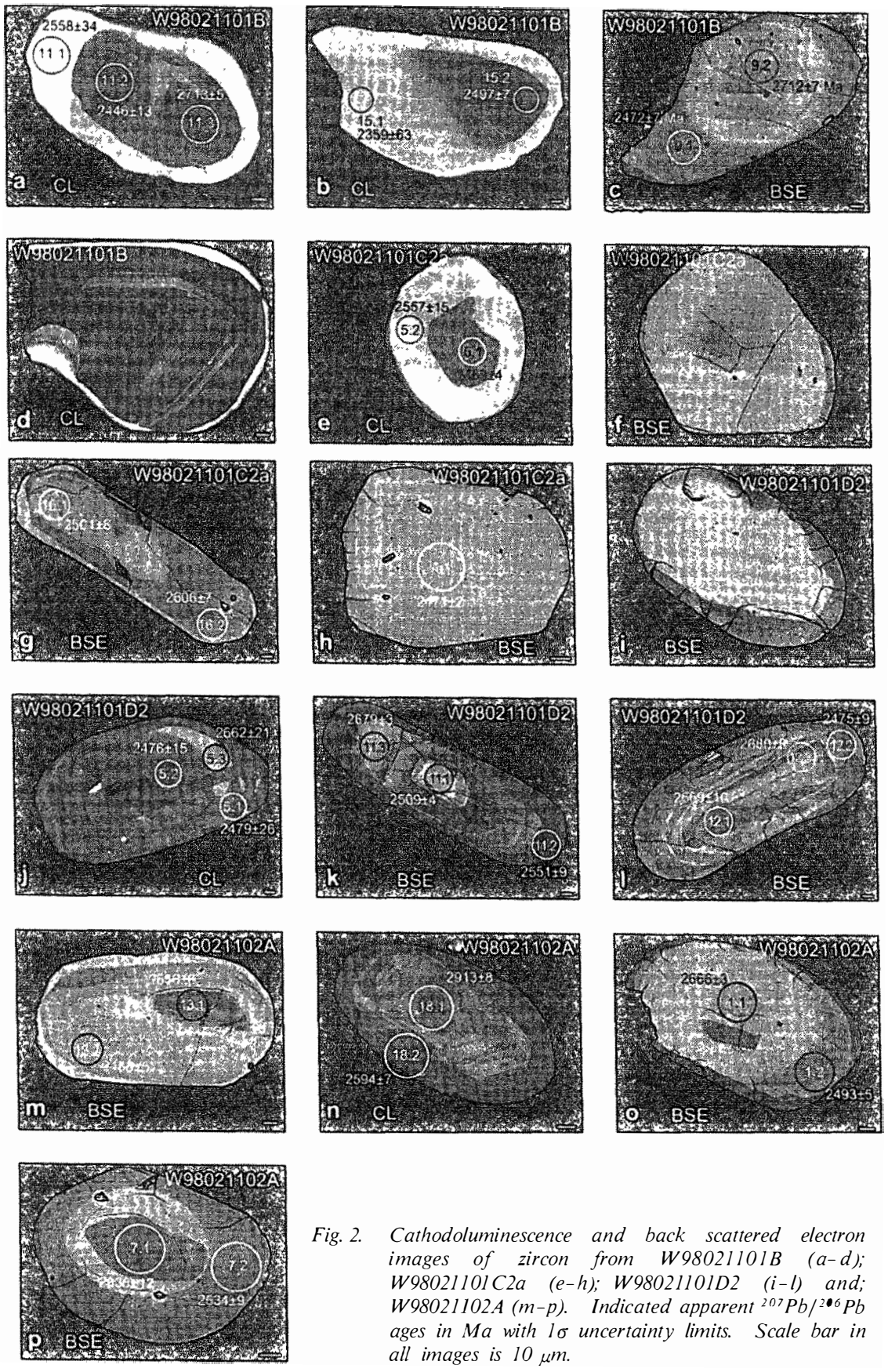

Fig. 2. Cathodoluminescence and back scattered electron images of zircon from W98021101B (a–d); W98021101C2a (e–h); W98021101D2 (i–l) and; W98021102A (m–p). Indicated apparent $^{207}Pb/^{206}Pb$ ages in Ma with 1σ uncertainty limits. Scale bar in all images is 10 μm.

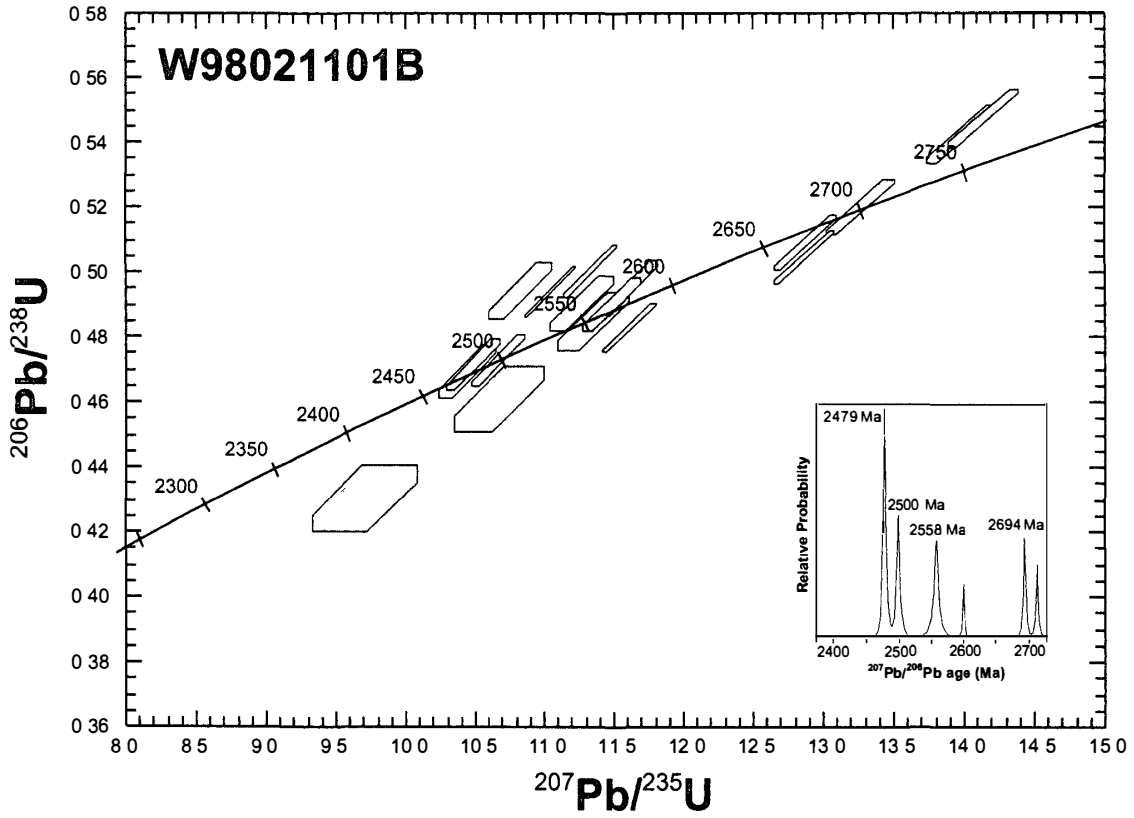

Fig 3 Conventional $^{206}Pb/^{238}U$-$^{207}Pb/^{235}U$ concordia diagram for 18 analyses of sample W98021101B using ^{204}Pb corrected SHRIMP data Analyses with U concentrations (below 20 ppm U) result in large analytical errors and are not plotted These data (analyses 4 1, 8 2, 11 1, 12 1, 13 1, 15 1, 16 1) are included within Table 2

Concordant and near concordant data define an older group at *ca* 2695 Ma These analyses are from variably preserved euhedrally zoned zircon cores (Figs 2a and c) A restricted Th/U ratio range between 0 2 and 1 1 for these analyses compared with ratios that range up to 4 6 for the main age group suggests significant U and Th mobilisation was associated with event(s) between *ca* 2550–2480 Ma A similar age component of *ca* 2660 Ma was derived from SHRIMP analysis of zircons from a quartz-feldspar gneiss on Tonagh Island by Shiraishi *et al* (1995)

5.2 Orthopyroxene garnet quartzofeldspathic mylonite (W98021101C2a)

A total of 21 zircon analyses were obtained for this sample A concordant and near concordant group of 15 analyses yield $^{207}Pb/^{206}Pb$ age group between *ca* 2515 Ma and 2470 Ma with a variable Th/U ratio between 0 1 and 1 6 This group does not define a statistically valid age representative of a single population (Fig 4) Four over lapping peaks defined on a probability distribution diagram for this main age group do not distinguish any clear age populations except perhaps for the strongest peak at *ca* 2508 Ma (Fig 4 inset)

These data are from structureless cores, cores that show an irregular and patchy BSE image response, recrystallised rims and rare structureless grains (*e.g* Fig 2h) Some grains have an incongruent age relationship between core and rim analyses (*e g.* Figs 2e and g)

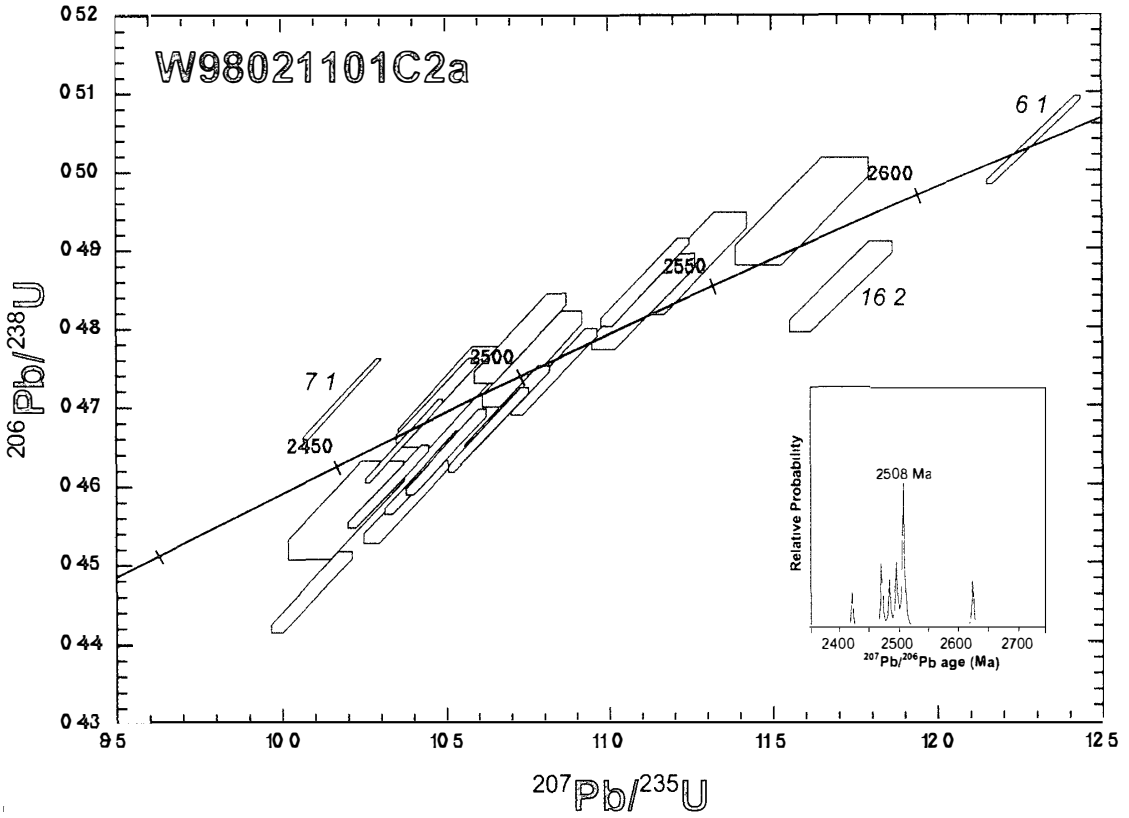

Fig 4 Conventional $^{206}Pb/^{238}U$-$^{207}Pb/^{235}U$ concordia diagram for 21 analyses of sample W98021101C2a using ^{204}Pb corrected SHRIMP data

In both examples the U content for the younger cores are relatively greater than for the corresponding rims The Th/U ratios for core and rim analyses in Fig 2e are nearly an order of degree different This is attributed to U and Th mobility associated with recrystallisation of the outer rim In contrast the patchy near structureless core and rim zircon that preserve a ghost relic euhedral zoning in Fig 2g have similar Th/U ratios These relationships reflect a selective Pb-loss in cores during a subsequent event which was possibly dependant of U content and probably on the degree of fluid interaction A spurious young and negatively discordant analysis (7 1) with extremely high U content (3746 ppm) is not considered as geologically significant due to a possible matrix-derived analytical bias (Black *et al*, 1991)

Two older analyses (6 1 and 16 2) record $^{207}Pb/^{206}Pb$ ages of 2625±2 Ma and 2606±7 Ma respectively and have consistent Th/U ratios of ~0 4 Analysis 16 2 is discordant and from a distinct zone within a rim which mantle a structureless core that yields a younger $^{207}Pb/^{206}Pb$ age of 2471±2 Ma (analysis 16 1 Fig 2g) The concordant analysis 6 1 is from a euhedrally zoned core

5 3 Orthopyroxene, quartzofeldspathic mylonite (W98021101D2)

A total of 22 zircon analyses were obtained for this sample Five concordant and near concordant analyses define a $^{207}Pb/^{206}Pb$ age of 2678±8 Ma (Fig 5) These analyses are from cores that show a disrupted euhedral zoning and cores with an irregular to

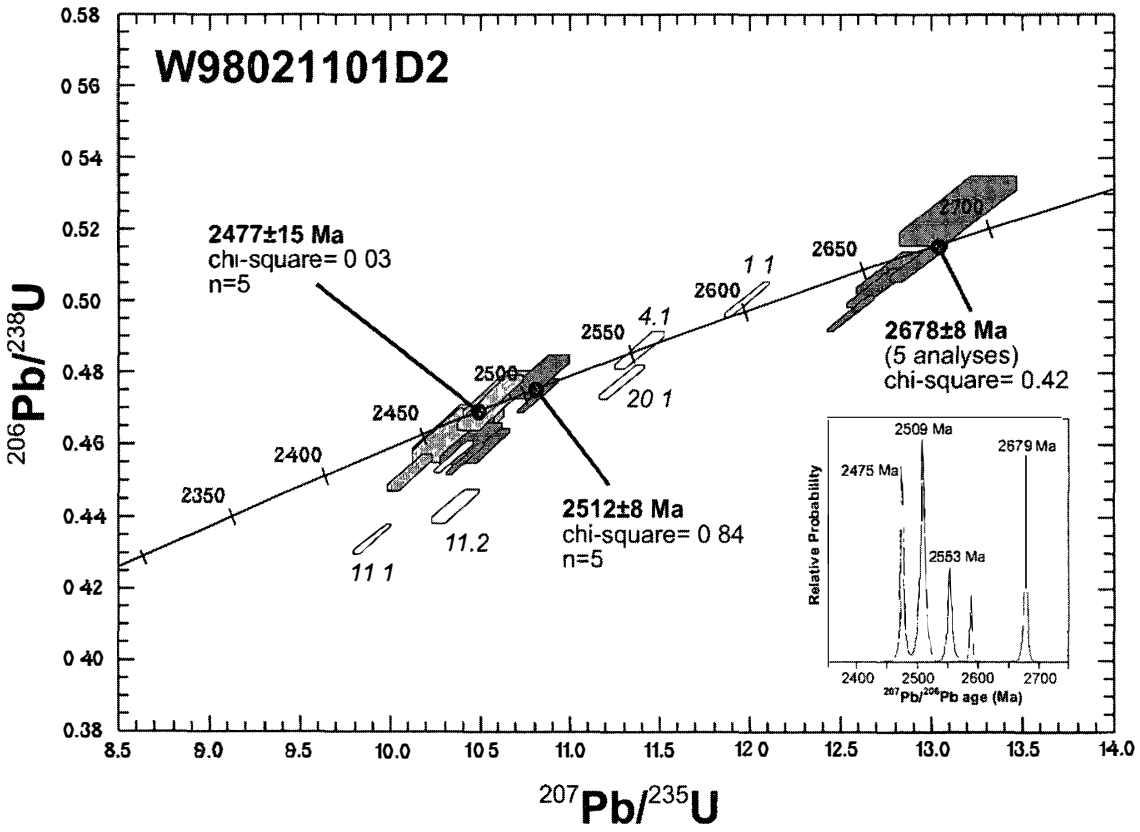

Fig 5 Conventional $^{206}Pb/^{238}U$-$^{207}Pb/^{235}U$ concordia diagram for 22 analyses of sample W98021101D2 using ^{204}Pb corrected SHRIMP data Weighted mean $^{207}Pb/^{206}Pb$ ages have errors reported at 95 percent confidence level

structureless BSE and Cl response In one core a euhedrally zoned portion yielded an indistinguishable $^{207}Pb/^{206}Pb$ age (within 1σ uncertainty limits) of 2680±6 Ma with a truncating structureless zircon which yielded a $^{207}Pb/^{206}Pb$ age of 2669± 10 Ma (Fig 2l) Structureless zircon that truncates and mantles both core associations yield an age of 2475±9 Ma (Fig 2l) The disparate nature of the zircon core associations with the same age are associated with variable Th/U ratios of between 0 2 and 1 9

Two weighted mean $^{207}Pb/^{206}Pb$ ages of 2512±8 Ma (5 analyses) and 2477±15 Ma (5 analyses) are defined within the main concordant and near concordant data group (Fig 5) and consistent with the defined age components resolved on the probability distribution diagram in Fig 5 inset Analyses that comprise these two populations are from structureless and partially preserved zoned rim and core zircon Two concordant and near concordant analyses (4 1 and 20 1) at *ca* 2550 Ma are consistent with concordant analyses in sample W98021101 B (Fig 3) and suggest these ages might be geologically significant An older near concordant analysis (1 1) possibly represents partial Pb-loss associated with the younger *ca* 2470–2500 Ma event(s) Minor recent Pb-loss is attributed to two normally discordant analyses (11 1 and 11 2), a core and rim analysis respectively from the same grain (Fig 2k and Fig 5)

5 4 Orthopyroxene, garnet ultramylonite (W98021102A)

Analyses for this sample define a reversly discordant to concordant array of $^{207}Pb/^{206}Pb$ ages between *ca* 2700 Ma and *ca* 2400 Ma (Fig 6) Analyses that comprise this data array are from cores preserving a relict euhedral zonation and wide structureless rims Older analyses of this data array tend to be from cores, which typically preserve relic primary zircon (*e g* Fig 2m-n) Two older core analyses with $^{207}Pb/^{206}Pb$ ages of 2801±10 Ma (spot 17 1) and 2913±8 Ma (spot 18 1) record relict Archaean components within the mylonitic rocks (Fig 6)

The reverse discordance of most analyses in this sample is not considered to be an artefact of poor calibration Sample W98021102A has a calibration uncertainty of 0 66% and was run in a single session with sample W98021101D2 which does not show any significant negative discordance in the data The low to moderate U concentration and Th/U ratios between 0 03 and 0 8 are comparatively low with respect to the other three samples and there is no evidence to indicate these zircons were metamict, suggesting apparent Pb-gain attributed to analytical bias in response to exceptional matrix characteristics is not tenable The reverse discordance is therefore due to excess radiogenic Pb or U and Th loss

Reverse discordance of data is not an uncommon phenomenon in the Napier Complex This has been variously attributed to excess radiogenic Pb associated with UHT metamorphism at 2820–2840 Ma, an event at or before *ca* 2225 Ma and a metamorphic event at *ca* 2400 Ma by Harley and Black (1997), Black *et al* (1986), Williams *et al*

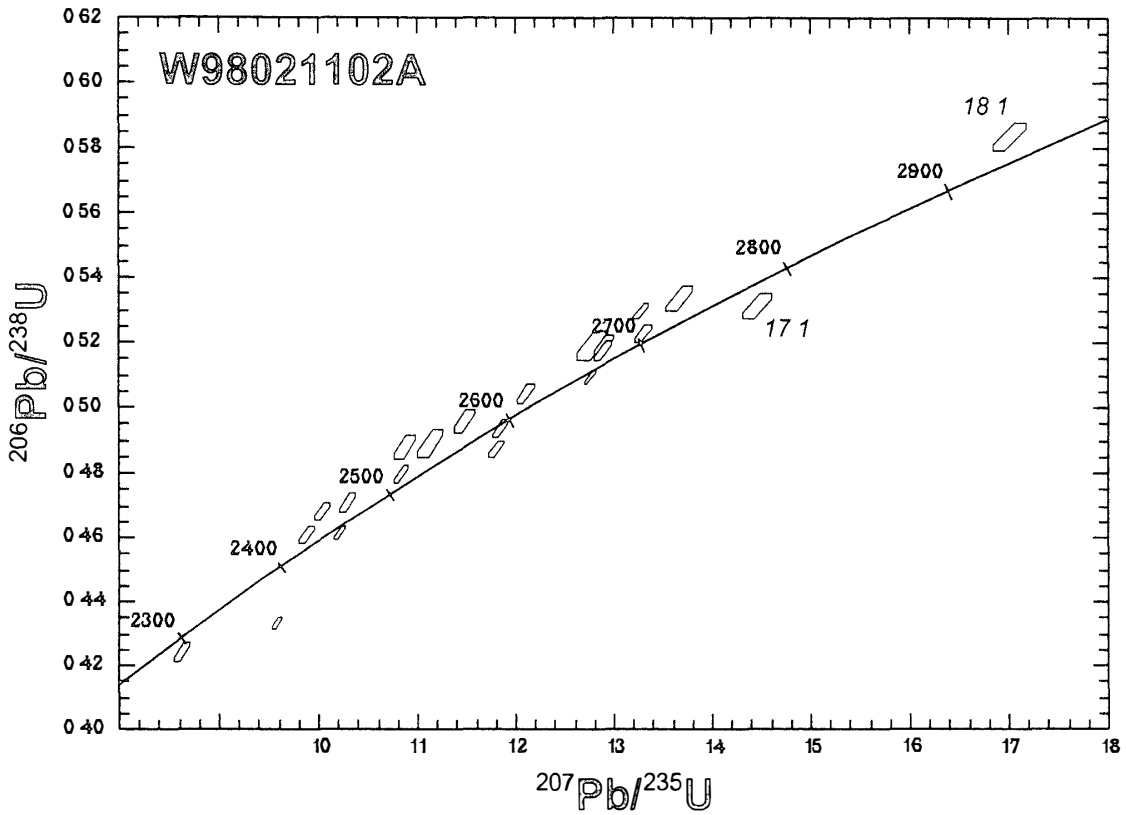

Fig 6 Conventional $^{206}Pb/^{238}U$-$^{207}Pb/^{235}U$ concordia diagram for 22 analyses of sample W98021102A using ^{204}Pb corrected SHRIMP data

(1984) respectively The reverse discordance of zircon data singularly present in one sample from three other closely located samples suggest this is only a local effect This sample is an ultramylonite and distinguished from the other three samples by a greater degree of dynamic recrystallisation late in the D6 shearing sequence It is suggested that entrainment of excess radiogenic Pb or removal of U and Th in zircon is attributed to the localised high strain associated with ultramylonitisation which possibly involved significant fluid ingress and isotopic mobilisation

6. Discussion

6 1 D_6 shearing between ca 2470–2550 Ma

Typical for all samples is the late textural association of biotite with respect to the main mylonitic fabric The preferred alignment of fine-grained biotite, biotite associated with the foliated pseudotachylite, the wrap-around fabrics on porphyroclasts and the relatively coarse grained biotite developed along fracture surfaces and pressure shadows of rounded and sub-rounded porphyroclasts indicates biotite formed pre- to syn- a secondary overprinting mylonitic fabric High temperatures were associated with this secondary hydrating mylonitisation event as indicated by the presence of late garnet with biotite as inclusions and as a relatively coarse-grained fracture filling and the apparent stability of orthopyroxene These textural associations suggest the rehydration of anhydrous mineral assemblages was associated with D_6 shearing and the presence of a fluid phase during shearing

Internal textures of zircon in BSE and CL images suggest the presence of a fluid was associated with the recrystallisation and annealing which record a near complete resetting of U-Pb isotopic systematics between *ca* 2550 and 2470 Ma The presence of outer rim zircon growth and associated recrystallised embayed zircon on the fractured surface of broken grains (*e.g.* Fig 2d) and the vein-like net work of healed fractures with $^{207}Pb/^{206}Pb$ ages of *ca.* 2480 Ma (*e g* Fig 2j) are consistent with an interpreted relationship between shearing and the timing of zircon recrystallisation and annealing Added support for the correlation of zircon recrystallisation and annealing with the timing of D_6 shearing is provided by the prominent reversely discordant zircon data from within a D_6 ultramylonite (sample W98021102A, Fig 6) This discordance has been shown to be a localised effect only recorded in zircon from the most strongly deformed sample, therefore indicating that Pb, U and Th mobility was associated with D_6 shearing and considered to have resulted from localised high strain and possible enhanced fluid ingress during this deformation

Only in one sample (W98021101D2) were weighted mean $^{207}Pb/^{206}Pb$ ages for the *ca* 2470–2550 interval able to be derived These indicated two possible distinct events at *ca* 2500 Ma and *ca* 2480 Ma Concordant and near concordant data in samples W98021101B and W98021101C2a are consistent with these two ages and suggest the presence of an earlier event at *ca* 2550 Ma Comparisons of probability distribution frequency diagrams for three samples show the presence of three distinct age populations at *ca* 2555 Ma, *ca* 2500 Ma and *ca* 2475 Ma (Fig 7) These three age populations within the 2470–2550 Ma interval may be related to a single Pb-loss event at *ca* 2480 Ma However, the consistent record of these age populations in three samples suggest they may be related to three distinct thermal events associated with reactivation of D_6 shear zones

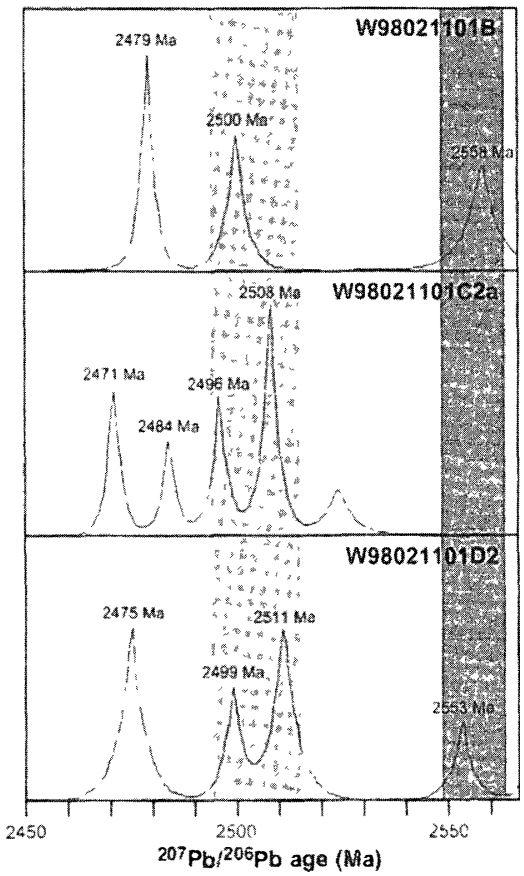

Fig 7 Comparative probability distribution diagrams for samples W98021101B, W98021101C2a and, W98021101D2 Shaded areas delimit consistent age populations between ca 2560 and 2470 Ma See text for discussion

Preservation of distinct age populations that record multiple events associated with near complete Pb-loss would require a variable duration and efficiency of Pb mobilisation The mylonite samples display a range of overprinting and strain variation textures at millimetre and centimetre scales which are attributed to successive mylonitisation and pseudotachylite stages These are consistent with a complex reactivation history involving multi-stage mylonitisation and pseudotacthylite development outlined for the D_6 shear zones by Toyoshima *et al* (1999) Therefore efficiency and domain variability of Pb-loss in zircon may be a consequence of localised strain state, fluid ingress and isotopic composition in addition to temperature and fluid composition considerations, all which may have varied between successive stages of deformation

Carson *et al* (2002a, b) and Shiraishi *et al* (1997) report similar results with concordant ages between *ca* 2550 and 2440 Ma from SHRIMP analysis of internally complex zircons from orthogneiss on Tonagh Island attributed to two separate events A four point whole-rock Sm-Nd isochron age of 2458±61 Ma obtained by Owada *et al* (1994) for samples with intercrystalline deformed granoblastic fabrics are considered to date the regional D_3-M_3 event These results indicate the 2470–2550 Ma events were pervasive through Tonagh Island and not restricted to the D_6 mylonite zones

6 2 The significance of the ca 2700 Ma ages

A weighted mean $^{207}Pb/^{206}Pb$ age of 2678±8 Ma (sample W98021101D2) is consistent with concordant and near concordant $^{207}Pb/^{206}Pb$ ages in sample W98021101B and a concentration of reversely discordant $^{207}Pb/^{206}Pb$ ages between *ca* 2640 Ma and *ca* 2700 Ma in sample W98021102A This *ca* 2680 Ma age is derived from variably preserved euhedrally zoned cores, structureless embayed zircon and structureless core and rim zircon (*e.g.* Figs 2a, c, g, j, k, l, m and p) A similar age of *ca* 2626±28 Ma were obtained by Carson *et al* (2002a) from oscillatory zoned cores of zircons from the orthogneiss on Tonagh Island These ages are considered to represent the timing of emplacement of the felsic intrusive protolith to the Tonogh Island orthogneiss based on a typical magmatic Th/U ratio for zircon analyses and the oscillatory zoned nature of the analysed cores (Carson *et al* , 2002a)

The significance of the *ca* 2680 Ma age for the D_6 mylonite is unclear Analyses which define this age population show a variable Th/U ratio (between 0 2 and 1 9) and are obtained from both structured and structureless zircon though all are from core zones In light of the results of Carson *et al* (2002a), this age may represent preserved relics of magmatic zircon associated with protolith emplacement of the orthogneiss

The presence of older Archaean components are indicated by an imprecise five point Sm-Nd isochron age of 3708±533 Ma, inherited zircons yielding SHRIMP $^{207}Pb/^{206}Pb$ ages of 3280 Ma, 3230 Ma and 2660 Ma and SHRIMP $^{207}Pb/^{206}Pb$ ages of 2801 and 2913 Ma (Owada *et al* , 1994, Shiraishi *et al* , 1997, this study respectively)

6 3. Implications for the timing of UHT metamorphism

The controversy over the timing of UHT metamorphism within the Napier Complex in part stems from the poor constraints of geochronological data within the relative deformation sequence and interpretation of the geochronological data from various geochronometers through a protracted series of granulite facies events between *ca* 3070 Ma and *ca* 2450 Ma To reiterate from the introduction there are currently two principal schools of thought in regard to the timing of UHT metamorphism, a pre- *ca* 2550–2590 Ma peak (Harley and Black 1997, Harley *et al* , 2001) or a peak associated with the predominant isotopic imprint at *ca* 2450–2500 Ma (DePaolo *et al* , 1982, Black *et al* , 1986, Asami *et al* , 1998, Carson *et al* , 2002a, b)

The relative timing of UHT metamorphism on Tonagh Island is synchronous with D_1, whereas D_2-D_6 deformation is associated with retrograde granulite facies conditions (Toyoshima *et al* , 1999) The timing of D_6 mylonitisation is constrained at *ca* 2470–2550 Ma by this study If the timing of UHT metamorphism is associated with the *ca* 2450–2500 Ma tectonothermal event then D_1-D_6 on Tonagh Island must be constrained within this same time interval Harley *et al* (2001) constrain UHT metamorphism to pre- *ca* 2550–2590 Ma and argue that the *ca* 2450–2500 Ma U-Pb ages record post metamorphic peak zircon growth and/or Pb loss associated with fluid infiltration and partial garnet break down This scenario is consistent with an earlier timing for D_1 and associated UHT metamorphism on Tonagh Island which was followed by retrogression through D_2-D_5 culminating with the development of the D_6 shear zones and fluid ingress at *ca* 2470–2550 Ma

7. Conclusion

The poly-phase D_6 mylonite zones on Tonagh Island developed late in the relative deformation history associated with the last high-grade event(s) to have affected the area, truncating all previous structures (Toyoshima *et al*, 1999) Recrystallisation and annealing associated with near complete Pb-loss in zircon from samples of the D_6 mylonite is attributed to fluid ingress and high temperatures associated with reactivation and over printing mylonite formation SHRIMP $^{207}Pb/^{206}Pb$ dates for these zircons constrain the timing of D_6 shearing and mylonite development to possibly three events at *ca* 2550 Ma, *ca* 2500 Ma and *ca* 2475 Ma An older $^{207}Pb/^{206}Pb$ age of 2678 ± 8 may represent inherited relics of magmatic zircon

The results of this study have wider implications for the regional tectonics of the Napier Complex The UHT metamorphic assemblages associated with D_1 fabrics on Tonagh Island are cut by the D_6 mylonite zones (Toyoshima, 1999) The constraints on the timing of D_6 to *ca* 2470–2550 Ma indicate that the UHT metamorphism was associated with an earlier event In a regional context, these results are consistent with models for pre- *ca* 2550 Ma UHT metamorphism

Acknowledgments

The authors wish to thank the expeditioners of JARE-39 and the crew of the icebreaker *Shirase* for their support and hospitality during the 1997–1998 field season WAC also thanks K Shiraishi and Y Motoyoshi of the National Institute of Polar Research for the invitation to participate in the SEAL (Structure and Evolution of East Antarctic Lithosphere) program We thank C J Carson and K Suzuki for critically assessing the manuscript Discussions with M T D Wingate and a subsequent review of an early draft of the manuscript are greatly appreciated by WAC Marion Marshall is thanked for sample and mount preparation Tectonics Special Research Centre Publication No 185

References

Asami, M, Suzuki, K, Grew, E S and Adachi M (1998) CHIME ages for granulites from the Napier Complex East Antarctica Polar Geosci, **11**, 172–199

Black, L P, James, P R and Harley, S L (1983) The geochronology, structure and metamorphism of early Archaean rocks at Fyfe Hills, Enderby Land, Antarctica Precambrian Res, **3**, 197–222

Black, L P and James, P R (1983) Geological history of the Archaean Napier Complex of Enderby Land Antarctic Earth Science, ed by R L Oliver *et al* Canberra, Australian Academy of Science 11–15

Black L P, Sheraton, J W and James, P R (1986) Late Archaean granites of the Napier Complex Enderby Land, Antarctica, a comparison of Rb-Sr, Sm-Nd and U-Pb isotopic systematics in a complex terrain Precambrian Res, **32**, 343–368

Black, L P, Kinny, P D and Sheraton, J W (1991) The difficulties of dating mafic dykes an Antarctic example Contrib Mineral Petrol, **109**, 183–194

Carson C J Ague, J J and Coath, C D (2002a) U-Pb geochronology from Tonagh Island East Antarctica implications for the timing of ultra-high temperature metamorphism of the Napier Complex Precambrian Res **116**, 237–263

Carson, C J , Ague, J J , Grove, M , Coath, C D and Harrison, T M (2002b) U-Pb isotopic behaviour of zircon during upper-amphibolite facies fluid infiltration in the Napier Complex, east Antarctica Earth Planet Sci Lett (in press)

Dallwitz, W B (1968) Coexisting sapphirine and quartz in granulites from Enderby Land, Antarctica Nature, **219**, 476–477

DePaolo, D J , Manton, W I , Grew, E S and Halpern, M (1982) Sm-Nd, Rb-Sr and U-Th-Pb systematics of granulite facies rocks from Fyfe Hills, Enderby Land, Antarctica Nature, **298**, 614–618

Ellis, D J (1980) Osumilite-saphirine-quartz granulites from Enderby Land, Antarctica *P-T* conditions of metamorphism, implications for garnet-cordierite equilibria and evolution of the deep crust Contrib Mineral Petrol , **74**, 201–210

Gebauer, D , Schertl, H P , Brix, M and Schreyer, W (1997) 35 Ma old ultrahigh-pressure metamorphism and evidence for very rapid exhumation in the Dora Maira Massif, Western Alps Lithos, **41**, 5–24

Grew, E S (1980) Osumilite in the sapphirine-quartz terrane of Enderby Land, Antarctica implications for osumilite petrogenesis in the granulite facies Am Mineral , **67**, 762–787

Grew, E S and Manton, W I (1979) Archean rocks in Antarctica 2 5 billion-year uranium-lead ages of pegmatites in Enderby Land Science, **206**, 443–445

Harley, S L (1985) Garnet-orthopyroxene bearing granulites from Enderby Land, Antarctica metamorphic pressure-temperature-time evolution of the Archaean Napier Complex J Petrol , **26**, 819–856

Harley, S L (1998) On the occurrence and characterization of ultrahigh-temperature crustal metamorphism What Drives Metamorphism and Metamorphic Reactions ?, ed by P J Treloar and P J O'Brien London, Geological Society, 81–107 (Geologocal Society Special Publication, No 138)

Harley, S L and Black, L P (1997) A revised Archaean chronology for the Napier Complex, Enderby Land, from SHRIMP ion-microprobe studies Antarct Sci , **9**, 74–91

Harley, S L and Hensen, B J (1990) Archaean and Proterozoic high-grade terranes of East Antarctica (40–80 degrees E), a case study of diversity in granulite facies metamorphism Metamorphism and Crustal Anatexis, ed by J R Ashworth and M Brown London, Unwin Hyman, 320–370

Harley, S L and Motoyoshi, Y (2000) Al zoning in orthopyroxene in a sapphirine quartzite evidence for >1120°C UHT metamorphism in the Napier Complex, Antarctica, and implications for the entropy of sapphrine Contrib Mineral Petrol , **138**, 293–307

Harley, S L , Kinny, P D , Snape, I and Black, L P (2001) Zircon chemistry and the definition of events in the Archaean granulite terrains 4th International Archaean Symposium 2001, Extended Abstracts, ed by K F Cassidy *et al* AGSO—Geoscience Australia, Record 2001/37, 511–513

Hokada, T , Osanai, Y , Toyoshima, T , Owada, M , Tsunogae, T and Crowe, W A (1999) Petrology and metamorphism of sapphirine-bearing aluminous gneisses from Tonagh Island in the Napier Complex, East Antarctica Polar Geosci , **12**, 49–70

James, P R and Black, L P (1981) A review of the structural evolution and geochronology of the Archaean Napier Complex of Enderby Land, Australian Antarctic Territory Archaean Geology, Second International Symposium, ed by J E Glover and D I Groves Perth, Geological Society of Australia Incorporated, 71–83

Motoyoshi, Y , Hensen, B J and Matsueda, H (1990) Metastable growth of corundum adjacent to quartz in a spinel-bearing quartzite from the Archaean Napier Complex, Antarctica J Metamorph Geol , **8**, 125–130

Nelson, D R (1997) Compilation of SHRIMP U-Pb zircon geochronology data, 1996 Geological Survey of Western Australia, Record, 1997/2 189 p

Osanai, Y , Toyoshima, T , Owada, M , Tsunogae, T , Hokada, T and Crowe, W A (1999) Geology of ultrahigh-temperature metamorphic rocks from Tonagh Island in the Napier Complex, East

Antarctica Polar Geosci **12** 1–28

Osanai, Y., Toyoshima, T. Owada, M., Tsunogae T., Hokada, T. Yoshimura Y., Miyamoto T., Motoyoshi, Y., Crowe, W. A., Harley, S. L., Kanao, M. and Iwate, M. (2001) Explanatory text of geological map of Tonagh Island Enderby Land, Antarctica Antarctic Geological Map Series Sheet 38, Tokyo National Institute of Polar Research 40 p

Owada M. Osanai, Y. and Kagami H. (1994) Isotopic equilibration age of Sm-Nd whole-rock system in the Napier Complex (Tonagh Island), East Antarctica Proc. NIPR Symp. Antarct. Geosci. **7**, 122–132

Owada, M., Osanai, Y., Toyoshima T. Tsunogae, T. Hokada, T. and Crowe W. A. (1999) Petrography and geochemistry of mafic and ultramafic rocks from Tonagh Island in the Napier Complex East Antarctica a preliminary report Polar Geosci., **12**, 87–100

Pidgeon R. T. (1992) Recrystallisation of oscillatory zoned zircon some geochronological and petrological implications Contrib. Mineral. Petrol., **110**, 463–472

Schaltegger U., Fanning, C. M. Guenther, D. Maurin, J. C. Schulmann, K. and Gebauer D. (1999) Growth, annealing and recrystallization of zircon and preservation of monazite in high-grade metamorphism conventional and in-situ U-Pb isotope, cathodoluminescence and microchemical evidence Contrib. Mineral. Petrol., **134** 186–201

Sheraton, J. W., Tingey, R. J. Black L. P., Offe L. A. and Ellis D. J. (1987) Geology of Enderby Land and western Kemp Land, Antarctica BMR Bull. **223**, 51 p

Shiraishi, K., Ellis D. J., Fanning, C. M., Hiroi, Y., Kagami H. and Motoyoshi Y. (1997) Re-examination of the metamorphic and protolith ages of the Rayner Complex, Antarctica, evidence for the Cambrian (Pan-African) regional metamorphic event The Antarctic Region Geological Evolution and Processes, ed. by C. A. Ricci Siena Terra Antarctica Publication 79–88

Sandiford M. and Wilson C. J. L. (1984) The structural evolution of the Fyfe Hills-Khmara Bay region, Enderby Land, East Antarctica Aust. J. Earth Sci. **31** 403–426

Toyoshima, T., Osanai Y. Owada, M. Tsunogae, T., Hokada, T. and Crowe, W. A. (1999) Deformation of ultrahigh-temperature metamorphic rocks from Tonagh Island in the Napier Complex, East Antarctica Polar Geosci. **12**, 29–48

Tsunogae, T., Osanai Y., Toyoshima, T. Owada M., Hokada, T. and Crowe, W. A. (1999) Metamorphic reactions and preliminary P-T estimates of ultrahigh-temperature mafic granulite from Tonagh Island in the Napier Complex East Antarctica Polar Geosci. **12**, 71–86

Vavra G., Gebauer, D., Schmid, R. and Compston W. (1996) Multiple zircon growth and recrystallisation during polyphase Late Carboniferous to Triassic metamorphism in granulites of the Ivrea Zone (southern Alps) an ion microprobe (SHRIMP) study Contrib. Mineral. Petrol., **122**, 337–358

Vavra, G., Schmid, R. and Gebauer, D. (1999) Internal morphology habit and U-Th-Pb microanalysis of amphibolite-to-granulite facies zircons geochronology of the Ivrea Zone (southern Alps) Contrib. Mineral. Petrol., **134**, 380–404

Williams, I. S. Compston W. Black, L. P., Ireland T. R. and Foster J. J. (1984) Unsupported radiogenic Pb in zircon a cause of anomalously high Pb-Pb U-Pb, and Th-Pb ages Contrib. Mineral. Petrol., **88**, 322–327

(Received April 1, 2002, Revised manuscript accepted May 31, 2002)